POD-BASED ESTIMATION OF THE FLOW FIELD FROM FREE-SURFACE VELOCITY IN THE BACKWARD-FACING STEP

T.D. Nguyen[1*] · **T.X. Dinh**[2] · **J.C. Wells**[1] · **P. Mokhasi**[3] · **D. Rempfer**[4]

[1]: Dept. of Civil Engineering, Ritsumeikan University, Japan, thien.duy.ng@gmail.com
[2]: Dept. of Mechanical Engineering, Ritsumeikan University, Japan
[3]: Wolfram Research Inc, United States
[4]: Dept. of Mechanical, Materials & Aerospace Engineering, Illinois Institute of Technology, United States

ABSTRACT

With a view to "nowcasting" of depth-scale flow fields in rivers, estuaries, and the near-coast, this work develops empirical "measurement models" that correlate velocity at a water surface to subsurface flow fields. Free-surface flow over a backstep, as simulated by LES, is chosen as a test case. Proper Orthogonal Decomposition (POD) is first applied to both subsurface and surface velocity fields from a "training data set", whence we develop regression models between the vectors of surface and subsurface POD coefficients. These models are then applied to estimate the subsurface flow field outside the training data based on virtual "measurements" of streamwise velocity along a streamwise line at the water surface. Good predictive capability is obtained in a region some 20 step heights downstream of the step that is characterized by strong upwellings.

INTRODUCTION

This paper applies measurement models developed by Mokhasi *et al.* [1], who were motivated by "micro-nowcasting" and back-casting of chemical release in a city, and the "multi-time" extensions reported by Nguyen *et al.* [2]. "Nowcasting" referred originally to detailed, short-term weather forecasting, e.g. to predict the development of thunderstorms. The mathematics are the same as a "traditional" forecasting system, and typically include a nonlinear Kalman Filter (KF) that continually updates the "current estimate" for the vector of variables that specify the state of the system (atmosphere, ocean, etc.) in the chosen dynamical model. Since such physical systems are chaotic, monitoring data must be continually fed back to keep the current estimate close to reality; in the KF this data is compared with the "current state" via a "measurement model". In the scenario of [1], data from sensors distributed through a cityscape would feed back on a KF designed to track the turbulent flow; then, based on the estimated flow field, chemical concentration measurements would be "back-tracked" to estimate release location(s). As a prototype problem, they considered unidirectional flow past a surface-mounted cube. The measurement models proposed in [1] develop an idea from the fluids engineering literature known as "stochastic estimation", in which one estimates a flow field, via its POD coefficients, based on a limited number of measurements, typically pressure at one or more surface points. The dominant example has been Linear Stochastic Estimation (LSE). For example, Taylor and Glauser [3] built a low dimensional pressure sensing and control system via POD and LSE for a flow between a backward facing ramp and an adjustable flap; Durgesh and Naughton [4] applied a multi-time delay LSE-POD that used pressure to estimate POD coefficients of an unsteady near wake flow.

We are motivated by nowcasting of environmental flows with a free surface, notably estuaries and rivers. Existing systems (e.g. the NYHOPS network, [5]) are typically based on sparse point measurements, and cannot resolve horizontal variations much finer than the river width. For the future, we expect that High Frequency radar and/or imaging methods will be able to monitor surface velocity over a certain area. Indeed, highly-resolved data on surface velocity were obtained as early as 1967 by large-format aerial photography when rising flood waters generated surface bubbles as "PIV tracers", and the patterns of surface divergence even allowed Kinoshita [6] to infer the instantaneous spatial structure of subsurface bedforms. With this justification we investigate here the use of data measured over a portion of free surface as input for stochastic estimation. In the context of stochastic estimation, the introduction of a free surface was the key novelty in our recent communication [7]. That work considered simulated flow over a sinusoidal bed, with a free surface modeled as a stress-free lid. To simplify analysis, we confined attention to the flow velocity in three vertical-streamwise planes, and built POD-based correlations for the subsurface flow based on "measured" surface velocity.

In this paper, we also use information on free-surface velocity as input for estimation models. However, we instead study the flow past a backstep as a prototype for a subaqueous dune. Such "bedforms" are important because of their form drag, and because of their key role in sediment dynamics. In addition, the current work applies the correct dynamical conditions at the free surface. The LES of the backward-facing step flow with a free-surface is followed by a brief mathematical introduction of POD. Next, single-time and multi-time POD-based estimations are described and the performances of the POD-based estimations are discussed.

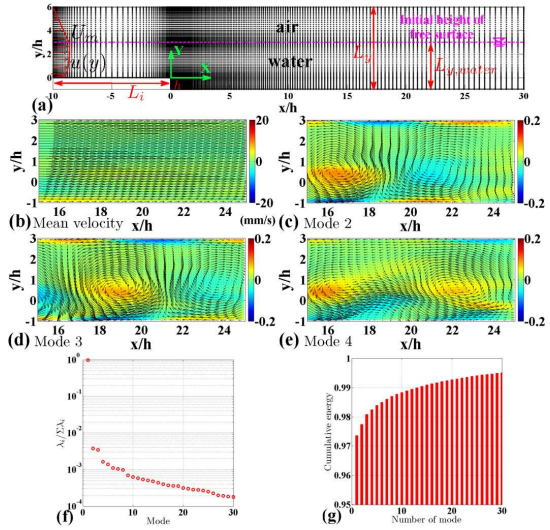

Figure 1. *(a)* LES simulation domain. POD decomposition to 1000 sub-surface velocity snapshots, *(b)* Averaged U, V velocity components, colour shows averaged W velocity component, *(c)-(e)* POD mode 2, 3 and 4, colour shows vorticity calculated from corresponding POD velocity basis function and normalized with the step height, $\omega_z^{'} = \omega_z h$, *(f)* energy spectra, *(g)* cumulative energy.

LARGE EDDY SIMULATION OF BACKWARD-FACING STEP

Let us first consider the specifications of the large eddy simulation of backward-facing step flow.

Figure 1*(a)* shows the simulation domain of the backward-facing step. The commercial software FLUENT 12.1 is used with the volume-of-fluid (VOF) to handle free-surface in this simulation. Step height h is 16.5 (mm). Computational domain has a streamwise length $L_x = 40h$ including an inlet streamwise length L_i of $10h$ prior to the edge. A spanwise width $L_z = \pi h$ and a vertical height L_y of the domain after the step is $7h$, of which a water flow depth $L_{y,water}$ is $4h$. A coordinate system is at the edge with the stream, vertical and span directions denoted by x, y and z respectively. The Reynolds number based on step height h and maximum mean inlet velocity U_m is 4400. A mean velocity profile $U(y)$ imposed at the inlet boundary of water-phase is taken from a flat-plate turbulent boundary layer [8], of which U_m is a maximum mean inlet velocity while a mean velocity profile for air-phase is linearly interpolated. A spectral synthesizer algorithm is applied to model the fluctuating velocity at the velocity inlet boundaries for this simulation. A pressure outlet condition is assigned for the downstream boundary. The top boundary condition of the simulation domain is shear-free while the bottom boundary condition is a no-slip, stationary wall. A periodic condition is assigned for the spanwise direction. The number of Cartesian grid points of the upstream domain is $50 \times 61 \times 18$ while that of the downstream domain is $151 \times 78 \times 18$. A uniform grid spacing is used in the spanwise direction while a non-uniform grid spacing is used in the vertical and horizontal directions with a finer mesh near the lower wall, the free-surface and the step. The range of grid spacings in wall units are $\triangle x^+_{min}/\triangle x^+_{max} = 10/90$, $\triangle y^+_{min}/\triangle y^+_{max} = 0.14/6.7$, and $\triangle z^+ = 34$ respectively based on the wall shear velocity $u_{\tau 0}$ taken at $x/h = -1$. The numerical simulation starts with 3D Reynolds-Averaged Navier-Stokes (RANS) with standard $k-\varepsilon$, SIMPLE pressure-velocity coupling and second order discretization. A converged flow field from RANS is then used as an initial condition to pursue the LES with Smagorinsky-Lilly model. A time step in this simulation is fixed at $\Delta t = 0.008 h/U_m$ which keeps the CFL number less than unity over the majority of the solution domain. The total simulation time of LES is $t_{total} = 555$ eddy turn-over times, where an eddy turn-over time is defined as h/U_m. About 273 eddy turn-over times, approximately 7 flow-through times, have been discarded for the passage of initial transients. A data set corresponding to 256 eddy turn-over times has been recorded to compute statistics. This data set consists of 1000 instantaneous snapshots of the three-component velocity fields of a vertical xy plane, with x/h ranging from 15 to 25 and y/h ranging from -1 to 3, in the mid-plane of the simulation domain. The time interval between each snapshot is $0.256 h/U_m$.

PROPER ORTHOGONAL DECOMPOSITION

The proper orthogonal decomposition (POD) is applied to the data set of instantaneous velocity snapshots of the BFS to reveal the dominant flow structures which capture most of the kinetic energy of the flow. The proper orthogonal decomposition of a velocity field $u(x, 0 \le t \le T)$, where T is a finite time interval, is given by

$$u(x,t) \cong \sum_{k=1}^{N'} \zeta_k(t)\psi_k(x), \tag{1}$$

where the maximal value of N' is the number of velocity fields N, $\zeta_k(t)$ are called the temporal POD coefficients and $\psi(x)$ are called the POD basis functions which are the eigenfunctions of the two-point correlation function $R(x,x')$ defined as

$$R(x,x') = \frac{1}{T}\int u(x,t)\cdot u(x',t)dt. \tag{2}$$

The basis functions are computed via an optimization problem leading to a Fredholm integral equation

$$\int R(x,x')\cdot\psi(x')dx' = \lambda\psi(x). \tag{3}$$

The eigenvalue λ associated with each POD mode is proportional to the kinetic energy contained in that mode. The decomposition yields statistically dominant flow structures in the few lowest-order POD modes, which capture most of the flow kinetic energy and are typically associated with large-scale structures.

In practical applications, the flow data are normally discrete; so integrals are computed by discrete summations. When the number of spatial sampling points exceeds the number N of velocity fields, as often encountered in computational

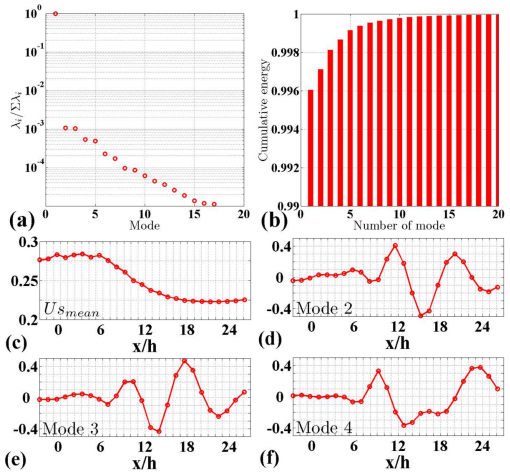

Figure 2. POD decomposition to 1000 free-surface velocity snapshots. *(a)* Energy spectra, *(b)* cumulative energy, *(c)* averaged velocity $U_{s,mean}$, *(d)-(f)* POD mode 2, 3 and 4.

fluid dynamic (CFD) and experimental applications, the snapshot POD [9] is more computationally efficient to determine the POD modes. In such circumstances, a set of instantaneous flow fields, often named "snapshots", is collected from experimental velocity fields (e.g. PIV) or CFD simulation. A correlation matrix is calculated as

$$C_{ij} = \frac{1}{N}\int u(x,t_i)\cdot u(x,t_j)dx, \tag{4}$$

where N is the number of PIV velocity snapshots. In order to compute the POD basis functions and temporal coefficients, let us first define α_{ki} as

$$\alpha_{ki} = \frac{\upsilon_i^k}{\sqrt{N\sum_{m=1}^{N}\sum_{r=1}^{N}\upsilon_m^k\upsilon_r^k C_{mr}}} \tag{5}$$

where υ_i^k is the ith element of the eigenvector υ^k corresponding to the eigenvalue λ_k of the correlation matrix C. The POD basis functions are then computed as

$$\psi_k(x) = \sum_{i=1}^{N}\alpha_{ki}u(x,t_i), \tag{6}$$

and the temporal coefficients as

$$\zeta_k(t) = \int u(x,t)\cdot\psi_k(x)dx = N\sum_{i=1}^{N}\alpha_{ki}C_{it}. \tag{7}$$

The eigenvectors and temporal coefficients of the POD decomposition satisfy the following orthogonality:

$$\int \psi_i(x)\cdot\psi_j(x)dx = \delta_{ij}, \tag{8}$$

$$\frac{1}{T}\int_0^T \zeta_i(t)\zeta_j(t)dt = \lambda_i\delta_{ij}. \tag{9}$$

where δ_{ij} is Kronecker delta.We perform a POD analysis to the data set of 1000 sub-surface velocity snapshots and examine the dominant flow structures. In addition to the three-component velocity fields, a strictly analogous POD of free-surface velocity is performed. The free-surface velocity is streamwise component while the sub-surface velocity field is three-component instantaneous velocity vectors corresponding to a vertical plane at the middle of the simulation domain.

In figure 1*(b)*, vectors are averaged U, V velocity components while colour is W velocity component computed from the data set. Figure 1*(c-e)* show mode 2, 3 and 4 of the POD sub-surface velocity decomposition. In figure 1*(f)*, the first POD mode contributes more than 97% the total kinetic energy of the flow while the second and the third POD modes have almost equal eigenvalues. In addition, a pair of vorticity structures revealed in mode 2 and mode 3 of POD basis functions has a very large-scale (order of h), by which its influence to the fluctuation of water surface is considerable. Figure 2 presents the POD decomposition of 1000 free-surface velocity snapshots. Except the first POD mode, POD modes from 2 to 9 appear in pair by their almost equal eigenvalues. Interestingly, the spatial centers of the vortices appearing in the POD sub-surface velocity mode 2 to 4 correspond to the streamwise locations of strong fluctuations in the free-surface POD modes. This result may indicate an interaction between the large-scale sub-surface turbulence structures and the free-surface. Such phenomena have been hardly seen by experiments or simulations with non-deformable top boundary.

POD-BASED ESTIMATION MODELS

In this section, we describe various POD-based estimation approaches, including single-time PCR-POD and KRR-POD [1] and multi-time PCR-POD and KRR-POD estimations [2], used to build measurement models.

Single-time PCR-POD

The PCR-POD technique estimates the POD coefficients $\zeta_k(t)$ through a linear relation with the events $s(t)$

$$\tilde{\zeta}_k(t) = \sum_{m=1}^{M} w_{km}s_{km}(t), \tag{10}$$

where M is the number of measurement points, and w are the coefficients of the PCR-POD estimation need to be determined. The number of PCR-POD estimation coefficients is equal to the number of measurement points, M. The objective of PCR-POD is to minimize the mean square error function $C(w)$ between the estimated and true POD coefficients

$$C(w) = min.\frac{1}{2}\sum_{i=1}^{N}\left(w_i s(t_i) - \zeta_i(t)\right)^2, \tag{11}$$

where $s(t_i)$ is the measurement event at time t_i from N measurements and $\zeta_i(t)$ is the ith POD coefficient of the velocity fields. Instead of deriving w by conventionally solving the linear system of derivative equation, the PCR-POD technique

looks for the coefficients that are the functions of the principal components of the free-surface velocity. Hence, a POD is performed on the events s,

$$s_r^{EN}(t) = \sum_{m=1}^{N_p} \beta_m^{EN}(t)\Gamma_{mr}^{EN}, \tag{12}$$

where Γ and β with superscript EN are the POD basis functions and POD coefficients derived from the given ensemble measurement events respectively (fig. 2). N_p is the number of modes used in the POD decomposition; its effect on the PCR-POD performance is discussed later. The orthogonality of Γ and β can be described as,

$$\beta_m^{EN}(t) = \sum_{r=1}^{N_p} s_r^{EN}(t)\Gamma_{mr}^{EN}. \tag{13}$$

A relationship between the POD coefficients of the velocity fields and the POD coefficients of the measurement events is built as

$$\tilde{\zeta}_k(t) = \mathbb{M}_{km}\beta_m(t), \tag{14}$$

where matrix of coefficients $\mathbb{M}$ is determined by solving the linear equation system expressed by

$$\mathbb{M}_{km} = \sum_{s=1}^{N_p} \zeta_{ks}^{EN}\omega_{sm}, \tag{15}$$

where the coefficient ω is related to the coefficient β by

$$\sum_{s=1}^{N_p} \beta_{ms}^{EN}\omega_{sr} = \delta_{mr}. \tag{16}$$

The final form is derived by substituting (13) and (16) into (14)

$$\tilde{\zeta}_k(t) = \sum_{r=1}^{N_p}\left(\sum_{i=1}^{N_p}\sum_{j=1}^{N_p}\left(\zeta_{ki}^{EN}\omega_{im}\sum_{m=1}^{N_p}\omega_{jm}s_{rj}^{EN}\right)\right)s_r(t). \tag{17}$$

This equation represents an estimation of the POD coefficients $\zeta_k(t)$ of the sub-surface velocity fields from the measurements of the free-surface velocity s through a linear relation.

Single time KRR-POD

In this technique, POD coefficients $\zeta_k(t)$ are approximated by a nonlinear relationship with the measurements $s(t)$

$$\tilde{\zeta}_k(t) = \sum_{j=1}^{N} w_j^k h_j(s), \tag{18}$$

where N is the number of snapshots, w^k are the estimation coefficients and h_j are nonlinear basis functions, most commonly radial basis functions (RBF). In this application, we use N vector values of measurement events s to make the regression. Therefore, the number of KRR-POD estimation coefficients for each ζ_k is N. Details of the RBF functions can be found in [1]. In this study, h is chosen to be a multi-quadric function which has the form

$$h_j(s) = \phi(s,s_j) = \sqrt{1+\varepsilon^2\left\|s-s_j\right\|_2^2}, \tag{19}$$

where ε is a scaling parameter and $\left\|s-s_j\right\|_2^2$ is the Euclidean distance between the events s and s_j. The objective of KRR-POD is to minimize a cost function defined as

$$C(w) = \sum_{i=1}^{N}(\zeta_i - \tilde{\zeta}_i)^2 + \sum_{j=1}^{N}\beta_j w_j^2, \tag{20}$$

where regularization parameters β are added to penalize large coefficients w that could appear due to large random fluctuations in training set. These parameters need not be constant and are often optimally determined by cross-validation. In this work, however N is rather large, so we set $\beta_j = \beta\forall j$. The unknown coefficients w^k are computed by taking the derivative of (20) and setting to zero;

$$\frac{\partial C}{\partial w_j^k} = 2\sum_{i=1}^{N}(\tilde{\zeta}_i - \zeta_i)h_j(s_i) + 2\beta w_j^k = 0. \tag{21}$$

In terms of the RBF functions denoted as

$$H_{ij} = h_j(s_i) = \phi\left(\left\|s_i^{EN} - s_j^{EN}\right\|\right), \tag{22}$$

where the superscript EN indicates data from the ensemble, the coefficient w can be evaluated by solving a system of linear equations. The result written in matrix notation is

$$w_j = \left[H_{ij}^T H_{ij} + \beta I_{ij}\right]^{-1} H_{ij}^T \zeta_j, \tag{23}$$

where I denotes the identity matrix. Once the w coefficients are determined, one can substitute w into (18) to find the regression form of KRR-POD technique as

$$\tilde{\zeta}_k = \sum_{j=1}^{N} w_j\phi\left(\left\|s_j^{EN} - s\right\|\right). \tag{24}$$

This equation shows that one can estimate the POD coefficients $\zeta(t)$ of the velocity fields from the measurements $s(t)$.

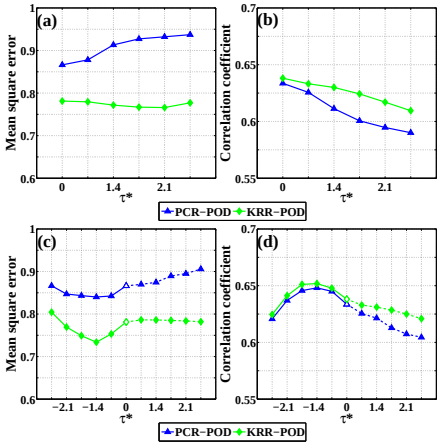

Figure 3. Comparison between multi-time PCR-POD and KRR-POD, *(a)* MSE, *(b)* CC by using both of the past and future information of free-surface velocity, *(c)* MSE, *(d)* CC by using the past information *(solid)* and the future information *(dashed)* of free-surface velocity.

Multi-time POD-based estimation approach

In the previous sections, the instantaneous POD coefficients of the velocity fields are estimated by using the measurement events at a single time. The multi-time PCR-POD and KRR-POD estimations [2] use the past and/or future information of measurement events to estimate the temporal POD coefficients of velocity fields. In this case, the POD coefficients of the velocity fields at time t are estimated by using conditional averages as

$$\tilde{\zeta}_k(t) = \left\langle \zeta_k(t) \mid s(t'), t-T \le t' \le t \right\rangle, \tag{25}$$

$$\tilde{\zeta}_k(t) = \left\langle \zeta_k(t) \mid s(t'), t \le t' \le t+T \right\rangle, \tag{26}$$

$$\tilde{\zeta}_k(t) = \left\langle \zeta_k(t) \mid s(t'), t-T \le t' \le t+T \right\rangle, \tag{27}$$

where subscript k denotes the POD mode, and T is the duration of the temporal window of measurement events used in the multi-time estimation. Equation (25) and (26) express that the past (future) information of the free-surface velocity is used separately, while (27) specifies that the past and future information of the free-surface velocity are combined. The implementations of multi-time PCR-POD and KRR-POD are similar to the single-time approaches, except that the matrix of event s is now expanded to include the measurement events from the past and/or future. Compared to the single-time estimations, the number of estimation coefficients of the multi-time PCR-POD approach increases in proportion to an increase in the time duration while that of the multi-time KRR-POD approach is constant.

RESULTS AND DISCUSSIONS

The multi-time PCR-POD and KRR-POD estimations have been applied to the BFS flow.The performances of these estimations has been compared via mean-square errors (MSE) and correlation coefficients (CC) between the "true" POD coefficients, determined from the original velocity fields by projection onto ψ_k, and the estimated coefficients. The POD coefficients are firstly standardized by applying *z-score* normalization, which shifts and re-scales the signal to a mean of zero and a standard deviation of one. The normalized POD coefficients the have the same standard deviation that gives an unbiased estimation to any POD coefficient [1]). The mean-square errors between the true and estimated POD coefficients, ζ and $\tilde{\zeta}$ respectively, are calculated by

$$\varepsilon^2 = \frac{1}{NN_v} \sum_{t=1}^{N} \sum_{k=1}^{N_v} \left(\tilde{\zeta}_k(t) - \zeta_k(t) \right)^2, \tag{28}$$

where N is the number of snapshots in the data set, N_v is the number of low-order POD coefficients, for example N_v is chosen as 4 in our application, or 1 when considering the error of a single mode. The correlation coefficient between the true and estimated POD coefficients, $\zeta_k(t)$ and $\tilde{\zeta}_k(t)$ respectively, are calculated by

$$C_k = \frac{\sum_{t=1}^{N} (\tilde{\zeta}_k(t) - <\tilde{\zeta}_k>)(\zeta_k(t) - <\zeta_k>)}{\sqrt{\sum_{t=1}^{N} \left(\tilde{\zeta}_k(t) - <\tilde{\zeta}_k>\right)^2} \sqrt{\sum_{t=1}^{N} (\zeta_k(t) - <\zeta_k>)^2}}, \tag{29}$$

where k indicates the POD mode, N is the number of snapshots in the data set and the operator $\langle . \rangle$ stands for the ensemble average.

The data set of 1000 sub-surface velocity fields and their corresponding free-surface velocity vectors have been divided into two sets of 500 snapshots. In this assessment, we first perform a POD decomposition on the first data set of the velocity fields, called the "ensemble", to obtain the spatial POD basis functions. Next, the time series of the four lowest-order temporal POD coefficients and corresponding free-surface velocity from the first set are used to build the estimation models and compute the estimation coefficients. Next, if the estimation coefficients determined from the ensemble operate on the free-surface velocity from another data set, one can approximately "predict" the values of POD coefficients of this set. The accuracy of prediction is computed by comparing the estimated POD coefficients with the actual POD coefficients. The non-dimensional duration τ^* is given by

$$\tau^* = \frac{TU_m}{h}, \tag{30}$$

where T is the time interval between each snapshot, U_m is the maximum inlet velocity, h is the step height of the BFS flow.

Figure 3*(a)* and *(b)* show the performances of the multi-time estimations PCR-POD and KRR-POD in which both the past and future information of the free-surface velocity are used. It is seen that an increase in duration τ^* reduces the accuracy of the multi-time estimations while $\tau^* = 0$, corresponding to the cases of single-times estimations, yields a slightly higher CC for the multi-time KRR-POD estimation. Figure 3*(c)* and *(d)* show the MSE and CC obtained by the multi-time estimation techniques in which the information from the past and the future of the free-surface velocity is used separately. In our application, use of future information on

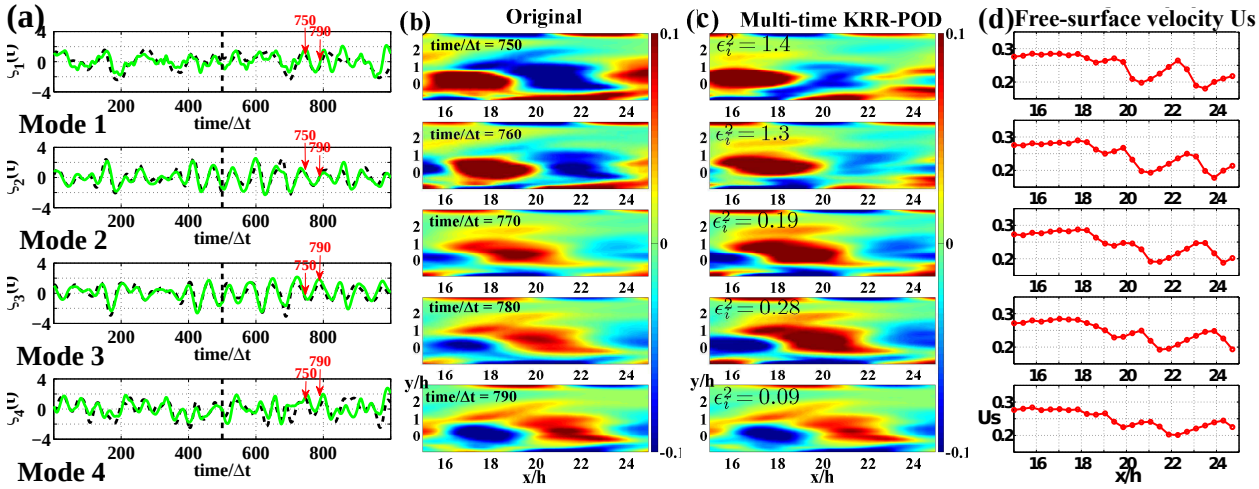

Figure 4. Estimation of sub-surface field from free-surface velocity by multi-time KRR-POD. *(a)* actual *(dashed)* and predicted *(solid)* POD coefficients, *(b)* original spanwise vorticity, *(c)* spanwise vorticity computed from predicted flow snapshots using *(d)* instantaneous free-surface velocity.

free-surface velocity events reduces the accuracy of prediction of all the estimation techniques. On the contrary, using past information with $\tau^* = -1.4$ $(I = -2)$ yields the best prediction for PCR-POD and KRR-POD, minimizing MSE and maximizing CC. This result reasonably suggests a phase relationship between the free-surface velocity and POD coefficients of the sub-surface velocity fields. From figure 3, it can be observed that the multi-time estimation KRR-POD, performs slightly better than PCR-POD in predicting the POD coefficients of sub-surface velocity fields if a certain duration of past information on free-surface velocity is included in the model. These performances demonstrate the capability of multi-time PCR-POD and KRR-POD estimations to successfully capture the relationship between the POD coefficients of sub-surface velocity fields and free-surface velocity events. Figure 4*(a)* compare the actual POD coefficients calculated from the original velocity fields with those from the KRR-POD estimation. From the predicted POD coefficients, corresponding estimates of velocity fields can be calculated. As an illustration, figure 4*(b)-(c)* shows five consecutive realizations of the spanwise vorticity, starting from $time/\triangle t = 750$, derived from the original and predicted velocity fields by using the low-order POD coefficients that are estimated by multi-time KRR-POD with $\tau^* = -1.4$ $(I = -2)$. The correspondingly instantaneous streamwise free-surface velocity U_s is also shown. For each instant, we calculate the MSE of POD coefficients, denoted as ε_i^2 and shown in figure 4*(c)*, between the true and predicted POD coefficients by applying (28) for a single time level. Referring to the temporal MSE of $\varepsilon^2 = 0.73$, these samples exhibit "typical" values of ε^2.

From these side-by-side comparisons, we assert that multi-time KRR-POD can provide good approximation to the sub-surface flow structures given the free-surface velocity events.

CONCLUSIONS

This paper develops the estimation models, based on POD analysis, that relate the free-surface velocity to low-order POD coefficients of the sub-surface velocity field of the BFS flow. We test the multi-time PCR-POD and KRR-POD estimations, in which the past and/or future information of the free-surface velocity is used. When there is a time lag between the POD coefficients and the given events, it is more efficient to employ multi-time estimations. Our proposed multi-time estimations have successfully captured the structures of the flow given a certain past information on free-surface velocity. Given the good predictive capability obtained from the region characterized by strong upwellings, we suggest that the multi-time estimations are practically useful to improve the capability for "nowcasting".

REFERENCES

[1] P. Mokhasi, D. Rempfer, and S. Kandala, "Predictive flow-field estimation," *Physica D*, vol. 238, no. 3, pp. 290–308, 2009.

[2] Nguyen, T.D., J. Wells, P. Mokhasi, and D. Rempfer, "POD-based estimations of the flow field from particle image velocimetry wall-gradient measurements in the backward-facing step flow," *Meas. Sci. Technol.*, vol. 21, no. 11, pp. 1–15, 2010a.

[3] J. Taylor and M. Glauser, "Towards practical flow sensing and control via POD and LSE based low-dimensional tools," *J. Fluids Eng.*, vol. 126, pp. 337–345, 2004.

[4] V. Durgesh and J. Naughton, "Multi-time-delay LSE-POD complementary approach applied to unsteady high-Reynolds-number near wake flow," *Exp. Fluids*, vol. 49, pp. 571–583, 2010.

[5] A. Blumberg, N. Georgas, *et al.*, "Quantifying uncertainty in estuarine and coastal ocean circulation modeling," *J. Hydraul. Eng.*, vol. 134, p. 403, 2008.

[6] R. Kinoshita, "An analysis of the movement of flood waters by aerial photography, concerning characteristics of turbulence and surface flow," *Photographic surveying*, vol. 6, pp. 1–17, 1967.

[7] Nguyen, T.D., N. Phan, J. Wells, P. Mokhasi, and D. Rempfer, "Prediction of the flowfield from free-surface measurements by POD-based estimation techniques," in *Proc. of 8th Int. Symp. ECOHYDRAULICS*, pp. 1–8, 2010.

[8] P. Spalart, "Direct simulation of a turbulent boundary layer up to Rθ= 1410," *J. Fluid Mech.*, vol. 187, pp. 61–98, 1988.

[9] L. Sirovich and M. Kirby, "Low-dimensional procedure for the characterization of human faces," *J. Opt. Soc. Am. A:*, vol. 4, no. 3, pp. 519–524, 1987.